PAPER

Catalytic CO$_2$ esterification with ethanol for the production of diethyl carbonate using optimized CeO$_2$ as catalyst†

Marco Buchmann, Martin Lucas [iD] and Marcus Rose [iD] *

The direct conversion of (bio)ethanol and CO$_2$ is a promising route to diethyl carbonate (DEC) since both reactants are cheap and originate from renewable resources in bioethanol production. In this work we present a detailed characterization and correlation between catalyst synthesis parameters and catalytic activity of pure ceria for DEC formation. An interaction between surface acidity and basicity as well as sufficiently high specific surface area is required for optimal catalytic activity which is obtained by using urea as the precipitation agent. Catalytic activity towards DEC formation is increased when adding both cerium nitrate solution and aqueous ammonia solution in a controlled manner at a pH of 10 at 50 °C for precipitation. When combining temperature-programmed desorption (TPD) experiments and catalytic testing, mainly weak basic sites appear to be relevant for the DEC formation.

Introduction

Diethyl carbonate (DEC) is a versatile compound with applications as solvent,[1,2] alkylating agent,[3,4] electrolyte,[5] monomer in polycarbonate synthesis[6–8] and fuel additive.[9] It is a colourless liquid which is biodegradable and non-toxic. The high oxygen content in combination with the mentioned properties renders DEC a very good replacement for MTBE as a fuel additive. Main production routes of linear organic carbonates typically suffer from using toxic and corrosive chemicals. At the moment, three commercial available synthesis routes are known: (I) direct reaction of alcohols and phosgene, (II) oxidative carbonylation using only O$_2$ and CO with a CuCl catalyst (Enichem process) and (III) also using O$_2$ and CO with an alkyl nitrite precursor and PdCl$_2$ as catalyst (Ube Industry).[10] An indirect use of CO$_2$ as starting material are the alcoholysis of urea[11,12] and trans-esterification of especially cyclic carbonates with alcohols.[13–16] In agreement with the principles of green chemistry and engineering a sustainable direct route in the DEC synthesis starting from bioethanol and CO$_2$ would be most favourable (Fig. 1). In the last two decades research was intensified in the field of the direct organic carbonate synthesis based on linear alcohols, mostly focusing on methanol to dimethyl carbonate (DMC), using CO$_2$ as substrate.[17] Especially the sustainable production of the starting materials, ethanol and CO$_2$, is crucial for the mentioned sustainable synthesis route. First generation

bioethanol production was a food-based biofuel which leads to a competition between food and fuel production.[18] Nowadays, with the second generation biofuels non-food raw material are in the focus.[19] The process is mainly based on lignocellulosic biomass and can also use industrial by-products, avoiding a competition between food and fuel production. The direct production of DMC and DEC has recently been summarized comprehensively.[20–24] The research focuses mainly on different catalysts (heterogeneous[25–29] and homogeneous[30,31]), different reactor types (continuous[32] and stirred batch tanks), and different starting materials like CO$_2$/ethanol or CO/H$_2$/ethanol.[32] Most promising and industrially relevant operating systems are based on heterogeneous catalysts.[33–35] Various groups investigated the influence of catalyst synthesis conditions and materials towards the DEC formation. The direct synthesis of DEC was reported for the first time by Yoshida *et al.* in 2006 using a commercially available CeO$_2$ catalyst.[36] In the following years different catalysts and syntheses routes were investigated. Self-prepared pure and mixed catalysts based on CeO$_2$ showed best catalytic activity

Technical University of Darmstadt, Department of Chemistry, Ernst-Berl-Institut für Technische und Makromolekulare Chemie, Alarich-Weiss-Straße 8, 64287 Darmstadt, Germany. E-mail: rose@tc2.tu-darmstadt.de

† Electronic supplementary information (ESI) available: Additional catalytic and analytical data. See DOI: 10.1039/d0cy01793k

Fig. 1 Schematic process flow sheet for the sustainable production of DEC from CO$_2$ and bioethanol based on the sugar fermentation with a direct subsequent conversion to DEC (reaction scheme).

towards DEC formation.[33,34,37] The catalysts were obtained using different precipitating agents, like aqueous ammonia solution or the citrate precipitation method. It was found that acid–base properties of the catalyst surface play an important role in catalytic activity.[38,39]

The addition of acid components like H_3PO_4 or $H_3PW_{12}O_{40}$ were shown to increase formation rates significantly.[38] The major challenge of the DEC synthesis is the strong thermodynamic limitation due to water formation during the process.[28] This problem can be overcome by reaction engineering approaches for *in situ* water removal.[33,40–42] Overall, a combination of a more active, reproducible and scalable catalyst in combination with the engineering for water removal are essential for industrial relevance of the direct production route towards DEC. CeO_2 based catalysts cannot only be used for direct carboxylation with linear alcohols but also play an very important role in the non-reductive transformation of CO_2 of cyclic carbonates,[43–46] different carbamates,[45,47–51] ureas,[45,50,52] and CO_2 based polymers.[6–8,53]

In this work, we focus on the catalyst preparation for the direct synthesis of DEC from ethanol and CO_2. For industrial applications a well-defined and reproducible catalyst synthesis is mandatory. The catalysts were prepared using either urea as precipitating agent, aqueous solutions of ammonia or sodium hydroxide. Synthesis parameters and catalyst pre-treatment were investigated to obtain an optimized catalyst.

Experimental section

Catalyst preparation

Cerium oxide and mixed oxide synthesis by urea precipitation. The desired amounts of precursor and additives ($Ce(NO_3)_3·6H_2O$ (Sigma-Aldrich, 99%), $ZrO(NO_3)_2·6H_2O$ (Sigma-Aldrich, 99%), $Sr(NO_3)_2$ (Sigma-Aldrich, 99.995%), $La(NO_3)_3·6H_2O$ (Sigma-Aldrich, 99.9%), $Al(NO_3)_3·9H_2O$ (Sigma-Aldrich, 99.997%), $Ca(NO_3)_2·4H_2O$ (Sigma-Aldrich, 99.997%), $Zn(NO_3)_2·6H_2O$ (AlfaAeser, 99%), $H_4SiW_{12}O_{40}$ (Sigma-Aldrich, 99%), $H_3PW_{12}O_{40}$ (AlfaAeser, 99.5%)) with an overall metal amount of 0.04 mol were dissolved in 250 mL deionized water. Urea (Sigma-Aldrich, ≥99.5%) in stoichiometric ratio 17 : 1 based on the overall metal content was added to the clear solution. The solution was stirred for 8 h at 100 °C. The white precipitate was filtered, washed three times with hot water, dried over night at 60 °C under vacuum and calcined for 4 h at the desired temperature.

Cerium oxide synthesis by continuous precipitation. A detailed scheme of the precipitation setup is shown in Fig. S9.† Cerium-(III)-nitrate ($Ce(NO_3)_3·6H_2O$; 18.92 g, 0.04 mol) was dissolved in 20 mL water and filled in a syringe placed in a computer controlled syringe pump. The solution was added dropwise with 0.5 ml min^{-1} to a solution containing either an aqueous ammonia or sodium hydroxide solution with the desired starting pH-value. The pH-value was controlled during the precipitation process and adjusted by a 25 wt% ammonia solution and a 2 M sodium hydroxide solution placed in the second syringe pump, respectively, and

automatically dosed based on a signal of a coupled pH electrode. Afterwards fully dispensed cerium nitrate solution was stirred vigorously for another two hours. The precipitate changed its colour from light red to purple as mentioned previously.[29,54] The purple precipitate was filtered, washed three times with hot water, dried over night at 60 °C under vacuum and calcined for 4 h at 600 °C.

Catalyst characterization

The specific surface of each sample was determined by nitrogen physisorption at −196 °C (Quantachrome, Quadrasorb Evo). Each sample was degassed for 10 h at 120 °C under vacuum. The specific surface area was calculated using the BET equation at p/p_0 = 0.02–0.15. X-ray powder diffraction was measured using a D2-Phaser (Bruker AXS) with Cu $K_{\alpha 1}$ radiation (30 kVA, 10 mA, λ = 1.5406 nm) with 2θ ranging from $20° \leq 2\theta \leq 90°$ and a scanning speed 0.005°/0.5 s. The sample was rotated during the measurement with 30 rpm. Acidic and basic properties were determined by temperature-programmed desorption (TPD) experiments using ammonia and carbon dioxide as probe molecules, respectively, and an Thermo Scientific Antaris IGS-System for gas analysis. For a typical measurement 0.1 g of the catalyst was loaded into a quartz tube, flushed with nitrogen and dried 2 h at 400 °C. The catalyst was loaded with a continuous stream of the probe molecule at 40 °C for 20 min. The physisorbed molecules were desorbed and flushed out using nitrogen for 20 min to ensure that only chemisorbed molecules remain on the sample. Chemisorbed probe molecules were desorbed by heating the catalyst to 500 °C with a rate of 10 K min^{-1}. The temperature of 500 °C was held for 30 min until full desorption of chemisorbed probe molecules occurred. XPS spectra were recorded on a SSX 100 ESCA spectrometer (Surface Science Laboratories Inc.) equipped with a monochromatic Al Kα X-ray source (9 kV, 10 mA). The X-ray spot size was 250–1000 µm. The binding energy scale of the system was calibrated using Au $4f_{7/2}$ = 84.0 eV and Cu $2p_{3/2}$ = 932.67 eV from foil samples. Charging of the powder samples was accounted for by setting the peak of the C 1s signal to 285.0 eV. A Shirley background was subtracted from all spectra. Peak fitting was performed with Casa XPS using 70/30 Gauss–Lorentz product functions. The degree of reduction of ceria was determined based on the ratio $Ce^{3+}/(Ce^{3+} + Ce^{4+})$ using the sum of integrated peaks for Ce^{3+} and Ce^{4+}, respectively.[55]

Catalytic testing

All experiments were carried out using a stainless steel pressure reactor (autoclave) with a total volume of 40 mL equipped with a magnetic stirrer bar and electric heating. In a standard procedure, 15.5 g of ethanol (20 mL, 337 mmol, Chemsolute, 99.9%) and 0.2 g catalyst were charged into the autoclave, purged and pressurized to 4.0 MPa of CO_2 (AirLiquide, 99.9995%). The reaction mixture was heated and mechanically stirred at the desired temperature for 4 h. After

This journal is © The Royal Society of Chemistry 2021

Catal. Sci. Technol., 2021, **11**, 1940–1948 | **1941**

the reaction, the reactor was cooled down in a water bath to ambient temperature and depressurized.

The liquid products were analysed by means of gas chromatography (Shimadzu, GC-2010 Plus) using a capillary column (Macherey–Nagel, Optima WAxPlus, 0.25 μm film, 0.25 mm diameter, 30 m length), n-tetradecane (Merck, >99.5%) as internal standard and equipped with a FID for substance measurement. The peaks in the chromatogram were identified by using the following pure substances: diethyl carbonate (Sigma-Aldrich, 99.9%), diethyl ether (Sigma-Aldrich, 99.9%), diethyl acetaldehyde (Sigma-Aldrich, 99%). Acetaldehyde was calculated according to the correlation to diethyl acetaldehyde given by Leibnitz and Struppe.[56]

Results and discussion

Catalyst characterization

The structure of the precipitate and the conversion to CeO_2 by calcination was investigated using X-ray powder diffraction (Fig. 2). It is remarkable that all precipitated samples were just filtered, washed with deionized water and dried overnight at 60 °C without any further calcination steps. According to the in situ XRD study by D'Angelo et al.[57] it can be seen that using urea as precipitating agent results in $Ce_2O(CO_3)_2 \cdot H_2O$ (PDF No. 00-043-0602, ICDD 2018). When using other basic precipitating agents like aqueous ammonia solution the precipitate only shows reflexes for CeO_2 even before the calcination step (Fig. 2, bottom). The same result occurs when using an aqueous sodium hydroxide solution as precipitating agent (see Fig. S1†). This leads to the assumption that during the precipitation with ammonia or sodium hydroxide solution the oxidation of cerium directly

occurs. The change in the oxidation state can also be observed by the colour change from slight red in the beginning of the precipitation to purple at the end.[29,54] The challenging sample preparation described by Tseng et al. showed the change by XPS measurements.

By calcining the urea-based precipitate under a constant air stream at different temperatures from 400–800 °C it is obvious that phase pure CeO_2 (PDF No. 00-034-0394, ICDD 2018) is obtained in a well controllable manner regarding the crystallite size. The reflexes get sharper with increasing temperature which indicates an increasing crystallite size which is in good agreement with literature.[29,36,58] According to this observation the average crystal sizes were calculated using the Debye Scherrer equation given below.

$$L = \frac{K \cdot \lambda}{\Delta(2\theta) \cdot \cos\theta_0}$$

K: Scherrer shape factor.

λ: wavelength X-ray radiation.

$\Delta(2\theta)$: line broadening due to the crystallite size.

θ_0: Bragg angle.

All calculated crystallite sizes are listed in Table 1. Larger crystallite sizes appear by increasing the calcination temperature. The opposite trend can be seen for the determination of specific surface area. It decreases drastically from 127.0 $m^2 g^{-1}$ at 400 °C to 5.3 $m^2 g^{-1}$ at 800 °C as expected due to crystallite growth and particle sintering.

The same trend is observed by comparing the crystallite sizes and the precipitating temperatures for the catalysts 4–13 (Table 1). Crystallite sizes increase with increasing precipitating temperature and pH value. Apart from comparing catalysts 6–8 it is obvious that catalyst 7 does not fit to the trend obtained by other temperature variation. Increasing the precipitation temperature or pH the crystal size increases also according to the corresponding lower value. Only for catalysts 6–8 the crystallite size decreases from 101 Å (20 °C) to 90 Å (50 °C) and increases to 123 Å (100 °C). Specific surface areas for all catalysts vary between 24.9 $m^2 g^{-1}$ and 79.0 $m^2 g^{-1}$ with no clear trend visible.

The ammonia and carbon dioxide uptake determined by temperature-programmed desorption (TPD) are indirectly proportional to the calcination temperature and hence, the crystallite size. Ammonia and carbon dioxide desorption begin at 50 °C and show a maximum at 100 °C pointing towards rather weak acid and basic sites (Fig. 3). Among other factors the amount and the strength of acid and basic sites affect the catalytic activity of the tested catalysts. All results are shown in Table 2. Only for the sample calcined at 400 °C calcination temperature and CO_2 as probe molecule two desorption peaks are present (Fig. 3, top).

The peak at higher temperature (400–600 °C) can be considered an artefact and be attributed to incorporated carbonate-species left in the catalyst due to incomplete calcination. The TPD is measured up to a temperature of 600 °C, whereas the catalyst is only calcined at 400 °C.
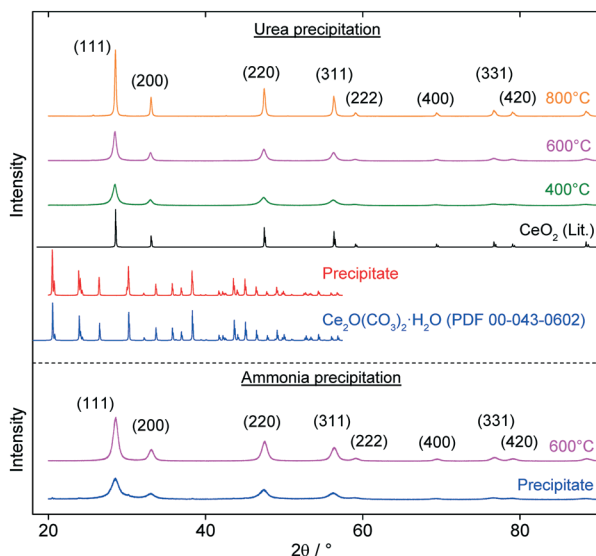

Fig. 2 Comparison of powder XRD pattern of CeO_2 precipitated from cerium(III) nitrate with urea (upper section) and ammonia solution (bottom section) and the influence of different calcination temperatures on the crystallite size.

Table 1 Synthesis parameters, specific surface area and acidic and basic properties of the synthesized CeO_2 catalysts

#	Precipitating agent	pH value	Precipitating temperature °C	Calcination temperature °C	CO_2 uptake μmol g^{-1}	NH_3 uptake μmol g^{-1}	Crystallite size Å	BET surface area m^2 g^{-1}
1	Urea	—	100	400	349.0	261.8	114.2	127.0
2	Urea	—	100	600	56.4	158.2	155.1	65.0
3	Urea	—	100	800	5.4	2.0	339.2	5.3
4	NH_4OH	9	20	600	98.6	102.7	105.1	57.1
5	NH_4OH	9	50	600	74.5	106.2	135.2	42.7
6	NH_4OH	10	20	600	91.8	118.1	101.9	57.3
7	NH_4OH	10	50	600	117.6	187.8	90.7	70.5
8	NH_4OH	10	100	600	92.6	119.9	123.4	54.1
9	NH_4OH	11	50	600	125.3	154.0	102.2	79.0
10	NaOH	9	20	600	111.4	144.4	107.7	60.5
11	NaOH	9	50	600	82.8	142.0	111.0	52.1
12	NaOH	10	20	600	116.3	100.3	108.1	45.1
13	NaOH	10	50	600	133.1	50.1	159.5	24.9

Hence, this peak can be ignored as basic site. But it is relevant that despite the XRD showed small crystallites of CeO_2 apparently there is a certain amount of carbonate species still present that only decompose at higher temperature.

This is in good agreement with works by D'Angelo et al.[57] and Janoš et al.[59] where they studied in detail the oxidation behaviour of $Ce_2O(CO_3)_2 \cdot H_2O$. Measured by TGA the oxidation can be prolonged up to 500 °C.

In comparison, at higher calcination temperatures only weak basic sites are identified by CO_2 TPD. The overall amount of basic sites decreases drastically with increasing calcination temperature (see Fig. S1†). Not only the amount but also the strength of the basic sites changes slightly from 120 °C (calc. 400 °C) to 165 °C (calc. 600 °C) and 140 °C (calc. 800 °C). Using NH_3 as probe molecule to characterize acid

sites it can be seen that for 400 °C and 600 °C calcination temperature only one broad desorption peak appears. This indicates only one kind of acid sites present on the catalyst. As shown from NH_3 TPD the total amount of acid sites decreases drastically with increasing calcination temperature.

In order to obtain more information on catalyst surface configuration X-ray photoelectron spectroscopy (XPS) was conducted. Fig. 4 shows the Ce3d spectra of two self-prepared CeO_2 catalysts. The indications made with sets of u and v assigned peaks correspond to two peaks of spin–orbit splitting of $3d_{3/2}$ and $3d_{5/2}$ electrons.[60] Different oxidation states in the catalyst surface can be differentiated by their respective line shapes in their final states $Ce^{3+} = U^0 + U' + V^0 + V'$ and $Ce^{4+} = U + U'' + U''' + V + V'' + V'''$. After peak integration the relation between Ce^{3+} and Ce^{4+} shows the reduction state at the surface. The urea precipitated catalyst (entry 2, Table 1) shows Ce^{3+}/Ce^{4+} of 29% whereas the ammonia precipitated catalyst (entry 7, Table 1) shows Ce^{3+}/Ce^{4+} of 43%. As shown by Boaro et al.[61] and Stoian et al.[62] a higher degree of reduction leads to more surface defects in CeO_2 surface structure and further on to a higher CO_2 uptake. This can be confirmed by our CO_2-TPD measurements shown before.

Catalytic tasting

In order to find the optimal catalyst for DEC formation different calcination temperatures (see Fig. S2†), catalyst compositions (see Fig. S3†) and additives (see Fig. S4†) were initially screened.
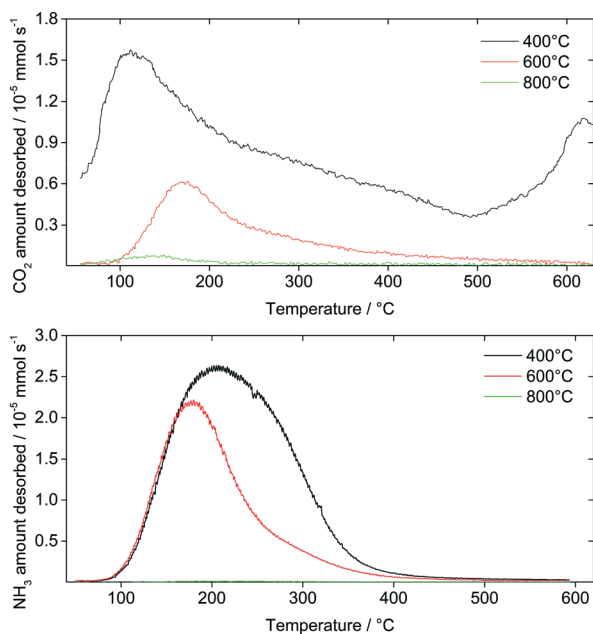

Fig. 3 CO_2-/NH_3-TPD profiles of CeO_2 (precipitation with urea) calcined at different temperatures. All catalysts were heated to 873 K and held at the temperature until no further desorption of the probe gas.

Table 2 Influence of the calcination temperature on the catalytic activity towards DEC formation

#	Calcination temperature	Concentration/mol L^{-1}		
		DEC	DEAA	AA
1	400 °C	0.0064	0.0022	0.0004
2	600 °C	0.0194	0.0005	—
3	800 °C	0.0008	—	—

Reaction conditions: 337 mmol ethanol, 0.2 g catalyst, 40 bar CO_2, 120 °C, 4 h reaction time.
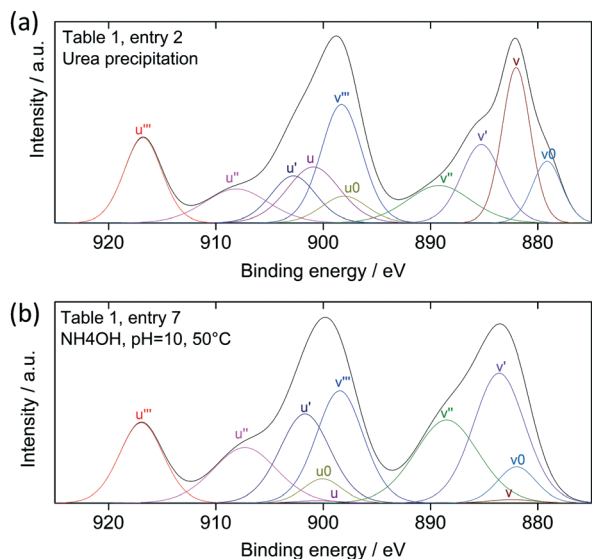
Fig. 4 XPS spectra of (a) CeO_2 prepared by urea precipitation method (entry 2, Table 1) and (b) CeO_2 prepared by ammonia precipitation method at pH 10 and 50 °C (entry 7, Table 1).

By comparing the results, the optimal catalyst is a pure CeO_2 catalyst precipitated with urea at 100 °C and subsequent calcination at 600 °C for 4 h. All additives and mixed oxides based on CeO_2 in order to increase acid and basic properties of the catalyst did not exceed the catalytic activity of pure microcrystalline CeO_2. Afterwards the optimal reaction conditions were evaluated by varying reaction time, initial CO_2 pressure, reaction temperature and the substrate-catalyst ratio. Detailed information on the kinetics, pressure and catalyst mass-dependence can be found in Fig. S5–S7.† It is obvious that the CO_2 pressure only has a minor influence (Fig. S6†) with an optimum at 40 bar. The reaction is not limited by mass transfer limitations as indicated by catalyst mass variation (Fig. S7†). Hence, optimal reaction conditions to evaluate catalytic activity without any thermodynamic, kinetic or mass transfer limitations are 40 bar initial CO_2 pressure, 120 °C, 4 h reaction time and 0.2 g catalyst. By comparing activity and selectivity of all synthesized catalysts and additives pure CeO_2 shows the best performance towards DEC formation. Finally, the reproducibility of the catalyst synthesis (by urea precipitation) is very high based on the variations on the catalytic performance. Reaction rates and by-product formation show only negligible deviations. Detailed information is shown in Fig. S8.† All graphics concerning catalytic activity measurements (Fig. 5–7) are plotted with total produced amount of DEC instead of the concentration additionally in Fig. S10† for a direct comparison with previous literature reports.

As shown before and agreeing with our results (see Table 2) the catalytic activity of ceria catalysts for the synthesis of linear organic carbonates cannot be directly correlated to the amount of acid and basic sites on the catalyst nor the available specific surface area.[26,29,39] Our experiments show that the highest reaction rates were obtained using the catalyst with a calcination temperature of
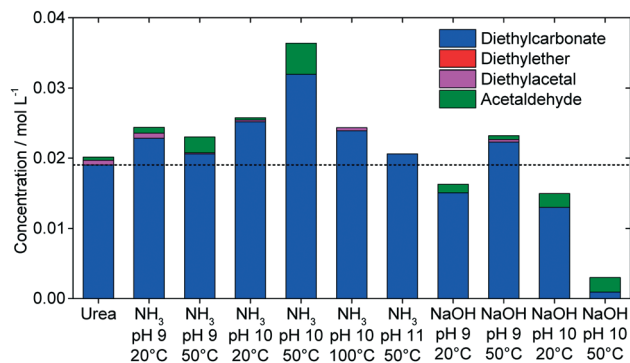

Fig. 5 Comparison of the influence of different precipitating agents and catalyst synthesis conditions on the catalytic activity towards DEC formation. Reaction conditions: 337 mmol ethanol, 0.2 g catalyst, 40 bar CO_2, 120 °C, 4 h reaction time.

600 °C. This catalyst does not show the highest amounts of acid and basic sites and not the highest specific surface area compared to all tested catalysts (Fig. S2†). As discussed in literature the reactivity and amount of active sites on the CeO_2 surface strongly depends on the available oxygen vacancies (OV) and crystallite shapes.[61,63–65] Especially the OVs on our catalyst seem to have a huge influence. The optimal surface texture is apparently obtained at 600 °C calcination temperature. Urea is used as precipitating agent due to its property to release ammonia at around 90 °C in an aqueous solution. All substrates are fully dissolved which lead to a very high dispersed and texturally well-defined precipitate. For a high reproducibility and scale-up of the catalyst preparation method a pH-value controlled precipitation and a direct use of ammonia and sodium hydroxide was used to improve and establish a reliable catalyst synthesis. The results of the catalytic activity measurements are shown in Fig. 5. Using an aqueous ammonia solution as precipitating agent leads to an increase in catalytic activity. The highest activity is achieved at a pH of 10 and 50 °C precipitation temperature.

Noteworthy, using this catalyst the highest amount of acetaldehyde as oxidized by-product is formed. This indicates
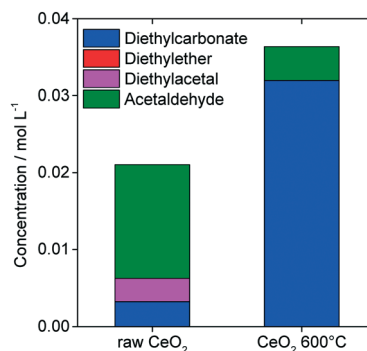

Fig. 6 Comparison of catalytic activity of fresh precipitate without any calcination and after precipitation on the DEC formation. Reaction conditions: 337 mmol ethanol, 0.2 g catalyst, 40 bar CO_2, 120 °C, 4 h reaction time.
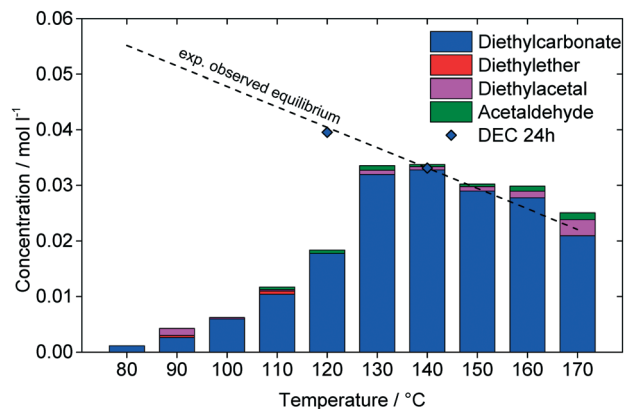
Fig. 7 Temperature dependence of the reaction showing the thermodynamic limitation of DEC formation after a certain reaction time or at higher temperatures with increased rates. Reaction conditions: 337 mmol ethanol, 0.2 g catalyst 2 (Table 1), 40 bar CO_2, 4 h reaction time.

a high amount of adsorbed oxygen on the catalyst surface resulting in the oxidative dehydrogenation of ethanol. In order to exclude O_2 impurities as reason for the acetaldehyde formation an experiment with 30 bar air instead of CO_2 was carried out and proved that the oxidative side-reaction is not catalytic under the applied conditions. The resulting amount of acetaldehyde was in the same order of magnitude as when using CO_2. This is in good agreement with oxidation experiments of ethanol to acetaldehyde with CeO_2 which starts at 200 °C.[66] Nevertheless, the increase of activity as measure of DEC yield compared to all other synthesized catalysts is up to 50%. Based on the catalysts characterization three main differences are obvious. Firstly, the best catalyst (NH_3, pH 10, 50 °C) shows the double amount of basic sites compared to the urea-precipitated catalyst. A feasible mechanism for the formation of dimethyl carbonate (DMC) from CO_2 and methanol has been proposed in literature by using *in situ* Raman, *in situ* IR and DRIFTS studies.[36,65,67] Carbon dioxide is activated on basic surface sites. Therefore, a higher amount of weak basic sites leads to higher reaction rates.[68] Wang *et al.* showed that a large number of strong basic sites is not favourable for the catalytic activity.[69] Secondly, the main difference is that the most active catalyst has the smallest mean crystallite size of all compared catalysts pointing towards the fact that the density of surface defects is a critical parameter. So far, no correlation between crystallite size and catalytic activity is obvious. Also, the conducted XPS measurements for two catalysts show a higher amount of reduced Ce^{3+} on the surface of the ammonia precipitated catalyst. Influence of Ce^{3+}/Ce^{4+}-ratio is discussed in literature where a higher amount of Ce^{3+} is attributed to a higher formation rate towards DMC formation.[68,72] Based on our observations we agree with these findings. In contrast, different reports in the field of DEC and DMC synthesis showed that a decrease in Ce^{3+}-concentration is more favourable together with an addition of heteroatoms such as aluminum, niobium and lanthanum.[34,73,74]

Table 3 summarizes results from previous reports and this work for the direct conversion of ethanol and carbon dioxide to DEC. For a direct comparison the catalyst productivity ($mmol_{DEC}\ mmol_{catalyst}^{-1}$ and $mmol_{DEC}\ g_{catalyst}^{-1}$) as well as the absolute amount of formed DEC ($mmol_{DEC}$) was extracted from the data for comparison. The maximum productivity without using a dehydration agent like butylene oxide (BO) or propylene oxide (PO) of 6.40 $mmol_{DEC}\ mmol_{catalyst}^{-1}$ was obtained with a CeO_2 catalyst[36] while other reports did not exceed a productivity of 0.22 $mmol_{DEC}\ mmol_{catalyst}^{-1}$.[36] Furthermore a kinetic study for the production of DEC using a commercial CeO_2 catalyst showed the same equilibrium concentration but a remarkable lower catalytic activity of 0.13 $mmol_{DEC}\ mmol_{catalyst}^{-1}$ at 4 h reaction time.[13] Higher productivities were so far only reported using dehydration agents for chemical water removal to shift the reaction equilibrium. With our catalyst prepared *via* direct ammonia precipitation at 50 °C and pH 10 the highest productivity of 0.53 $mmol_{DEC}\ mmol_{catalyst}^{-1}$ was achieved considering the reaction conditions without water removal.

Comparing the DEC formation rate is only possible in a kinetically controlled range before reaching the thermodynamic equilibrium. Here, the formation rate increases from 0.07 mmol $g_{Kat}^{-1}\ h^{-1}$ at 90 °C to 0.80 mmol $g_{Kat}^{-1}\ h^{-1}$ at 120 °C. Compared to literature values using pure CeO_2 best reported catalytic activity is 2.5 mmol $g_{Kat}^{-1}\ h^{-1}$.[71] Here we assume that reactor geometry, spare volume and ethanol amount : reactor diameter-ratio have huge impact in the catalyst performance. A direct comparison between different experiments being reported in literature is quite challenging.

As shown before XRD measurements of fresh precipitated cerium oxide with aqueous ammonia solution indicates a direct formation of CeO_2. The major difference between not calcined and calcined CeO_2 is the sharpness and intensity of the XRD reflexes. Catalytic tests confirm the presence of catalytic active CeO_2 in both catalysts with the much higher activity for the calcined CeO_2 (Fig. 6).

By using the not calcined CeO_2 the reaction products are dominated by the formation of the oxidation products acetaldehyde and diethylacetal. The ability of promoting oxidation reactions decreases drastically after calcination. As mentioned before thermodynamic limitation due to the reaction equilibrium is the greatest challenge in the formation of linear aliphatic carbonate production. Temperature-dependant experiments (Fig. 7) show the interdependence of kinetic and thermodynamic influence.

Initially, increasing the temperature results in an increased reaction rate with increasing product yields. By reaching the equilibrium conversion under the given reaction conditions at 140 °C not the kinetic but the equilibrium conditions limit the maximal yields that can be obtained. The equilibrium limited reaction temperature at 140 °C after 4 h reaction time was further investigated by longer reaction times (Fig. 6, blue dot). The dashed line shows the trend of the experimentally observed equilibrium concentration based

This journal is © The Royal Society of Chemistry 2021

Catal. Sci. Technol., 2021, **11**, 1940–1948 | 1945

Table 3 Influence of various reaction parameters on the catalytic activity towards DEC formation based on previous reports and the current work

#	Catalyst	Reaction conditions	Productivity[a] mmol$_{DEC}$ mmol$_{cat}^{-1}$	mmol$_{DEC}$	mmol$_{DEC}$ g$_{cat}^{-1}$	Ref.
1	CeO_2[b]	200 mmol ethanol, 200 mmol CO_2, 2 h, 170 °C, 10 mg catalyst	6.40	0.42	42	36
2	CeO_2[c]	257 mmol ethanol, 50 bar CO_2, 2 h, 140 °C, 0.5 g catalyst	0.14	0.40	0.80	69
3	CeO_2[b]	100 mmol ethanol, 2 bar CO_2, 4 h, 150 °C, 0.17 g catalyst	0.02	0.02	0.12	40
4	CeO_2[b]	100 mmol ethanol, 2 bar CO_2, 4 h, 150 °C, 600 mmol ACN, 0.17 g catalyst	6.00[d]	6.00	35	40
5	CeO_2[b]	314 mmol ethanol, 45 bar CO_2, 23 h, 170 °C, 1.0 g catalyst	0.07	0.40	0.40	28
6	3% Nb_2O_5/CeO_2[c]	68.5 mmol ethanol, 50 bar CO_2, 3 h, 135 °C, 380 mg catalyst	0.18	0.39	1.03	34
7	$Ce_{0.8}Zr_{0.2}O_2$[c]	$n_{Ethanol}/n_{CO_2}$ = 3, CO_2 feed = 62 mmol h^{-1}, GHSV 3200 h^{-1}, 100 °C, 2.5 g catalyst	0.22	0.47	0.19	33
8	Cu–Ni/AC[c]	He (50 mL min^{-1}) incl. 2.4% ethanol + 1.1% CO_2, 90 °C, 13 bar, 0.5 g catalyst	Conv. 2.7%			37
9	CeO_2[c]	314 mmol ethanol, 45 bar CO_2, 19 mmol BO, 23 h. 170 °C, 1 g catalyst	0.40[d]	2.33	2.33	25
10	CeO_2[c]	314 mmol ethanol, 19 mmol BO, 45 bar CO_2, 180 °C, 25 h, 1.0 g catalyst	0.34[d]	1.98	1.98	29
11	CeO_2[b]	20 mmol ethanol, 100 mmol 2-cyanopyridine, 50 bar CO_2, 0.34 g catalyst	4.50[d]	9.00	26	42
12	CeO_2[c]	170 mmol ethanol, 140 mmol PO, 50 bar CO_2, 2 h, 150 °C, 400 mg catalyst	1.15[d]	2.67	6.69	70
13	CeO_2/SiO_2[c]	314 mmol ethanol, 19 mmol BO, 45 bar CO_2, 180 °C, 25 h, 1.0 g catalyst	0.13[d]	0.76	0.76	27
14	CeO_2[b]	0.03 g catalyst, 140 mmol ethanol, 5 MPa CO_2, 393 K, 20 min	0.18	0.03	1.03	71
15	CeO_2[b]	0.5 g catalyst, 2,2-DEP, 140 mmol ethanol, 5 MPa CO_2, 393 K, 20 min	4.50[d]	13.00	26	71
16	**CeO_2[c]**	**337 mmol ethanol, 40 bar CO_2, 4 h, 120 °C, 0.2 g catalyst**	**0.53**	**0.64**	**3.20**	**This work**

[a] In mmol$_{DEC}$ mmol$_{catalyst}^{-1}$ (this unit of productivity was chosen as the given reaction times in all previous studies vary significantly and not in all cases a limitation by thermodynamic equilibrium can be excluded). [b] Commercial available catalyst. [c] Self-prepared catalyst. [d] Using dehydration agent.

on the results of the 4 h reaction experiments from 140 °C to 170 °C. The two long term experiments at 120 °C and 140 °C fit very well in the observed reaction equilibrium. The detailed thermodynamic properties of the direct formation of DEC from CO_2 and ethanol were investigated by Leino et al.[28] They showed that the Gibbs energy at ambient temperature is positive ($\Delta rG_{298K}^{\theta}$ = 35.85 kJ mol^{-1}) which shows that the reaction does not occur spontaneous. Also, the Gibbs energy increases linearly with the reaction temperature ($\Delta rG_{373K}^{\theta}$ = 48.89 kJ mol^{-1}). This corresponds very well with our experimentally observed behaviour. Overall, this shows the strong influence of the equilibrium reaction severely limiting the degree of conversion and the DEC yield. Hence, besides an optimized catalyst with highest productivity also the water as by-product has to be removed during the reaction in order to further increase the overall productivity.

Conclusions

In this work we investigated the influence of CeO_2 catalyst preparation by various synthesis and pre-treatment parameters on the catalytic activity for the conversion of ethanol with CO_2 to diethyl carbonate. High amounts of acidic and basic sites on the catalyst surface and a high specific surface are not the only requirements to efficiently catalyse this reaction. Especially surface defects like oxygen vacancies and probably also partially reduced Ce_2O_3 surface species play an important role. An optimum in calcination temperature was found at 600 °C. Furthermore, the temperature dependant limitations were investigated to ensure that every catalyst was tested in the range of the kinetically controlled regime far off the equilibrium limitations. With an ammonia-precipitated CeO_2 at pH 10 and 50 °C an increase in catalytic activity of up to 50% was achieved. In comparison to previously reported catalysts it showed the highest reported productivity for the direct conversion of ethanol and CO_2 without removal of the by-product water to shift the reaction equilibrium. With this knowledge future optimization regarding the reaction engineering and water removal, e.g. by a membrane reactor for water pervaporation, an efficient process for the direct production of diethyl carbonate from bioethanol and CO_2 seems feasible.

Conflicts of interest

There are no conflicts to declare.

Acknowledgements

1946 | *Catal. Sci. Technol.*, 2021, **11**, 1940–1948

This journal is © The Royal Society of Chemistry 2021

References

1 B. Schäffner, S. P. Verevkin and A. Börner, *Chem. Unserer Zeit*, 2009, **43**, 12–21.

2 B. Schäffner, F. Schäffner, S. P. Verevkin and A. Börner, *Chem. Rev.*, 2010, **110**, 4554–4581.

3 S. Yuvaraj, V. V. Balasubramanian and M. Palanichamy, *Appl. Catal., A*, 1999, **176**, 111–117.

4 S. Udayakumar, A. Pandurangan and P. K. Sinha, *Appl. Catal., A*, 2004, **272**, 267–279.

5 N. Saqib, C. M. Ganim, A. E. Shelton and J. M. Porter, *J. Electrochem. Soc.*, 2018, **165**, A4051–A4057.

6 R. Zhou, J. Liu, L. Jia, X. Lü and Z. Song, *Inorg. Chem. Commun.*, 2018, **90**, 57–60.

7 M. Tamura, K. Ito, M. Honda, Y. Nakagawa, H. Sugimoto and K. Tomishige, *Sci. Rep.*, 2016, **6**, 24038.

8 Y. Gu, K. Matsuda, A. Nakayama, M. Tamura, Y. Nakagawa and K. Tomishige, *ACS Sustainable Chem. Eng.*, 2019, **7**, 6304–6315.

9 W. Fu, L. Song, T. Liu and Q. Lin, *Proc. Inst. Mech. Eng., Part D*, 2017, **233**, 249–262.

10 P. Ratnasamy and S. Darbha, in *Handbook of Heterogeneous Catalysis*, Wiley-VCH Verlag GmbH & Co. KGaA, 2008, DOI: 10.1002/9783527610044.hetcat0192.

11 K. Shukla and V. C. Srivastava, *Catal. Rev.: Sci. Eng.*, 2017, **59**, 1–43.

12 T.-W. Wu and I. L. Chien, *Ind. Eng. Chem. Res.*, 2020, **59**, 1234–1248.

13 M. Décultot, A. Ledoux, M.-C. Fournier-Salaün and L. Estel, *Chem. Eng. Res. Des.*, 2020, **161**, 1–10.

14 P. Kumar, V. C. Srivastava and I. M. Mishra, *Energy Fuels*, 2015, **29**, 2664–2675.

15 W. Deng, L. Shi, J. Yao and Z. Zhang, *Carbon Resour. Convers.*, 2019, **2**, 198–212.

16 K. Shukla and V. C. Srivastava, *Ind. Eng. Chem. Res.*, 2018, **57**, 12726–12735.

17 A. Swapnesh, V. C. Srivastava and I. D. Mall, *Chem. Eng. Technol.*, 2014, **37**, 1765–1777.

18 J. Hill, E. Nelson, D. Tilman, S. Polasky and D. Tiffany, *Proc. Natl. Acad. Sci. U. S. A.*, 2006, **103**, 11206–11210.

19 K. Robak and M. Balcerek, *Food Technol. Biotechnol.*, 2018, **56**, 174–187.

20 H.-Z. Tan, Z.-Q. Wang, Z.-N. Xu, J. Sun, Y.-P. Xu, Q.-S. Chen, Y. Chen and G.-C. Guo, *Catal. Today*, 2018, **316**, 2–12.

21 K. Shukla and V. C. Srivastava, *RSC Adv.*, 2016, **6**, 32624–32645.

22 K. Tomishige, Y. Gu, Y. Nakagawa and M. Tamura, *Front. Energy Res.*, 2020, **8**, 117.

23 K. Tomishige, Y. Gu, T. Chang, M. Tamura and Y. Nakagawa, *Mater. Today Sustainability*, 2020, **9**, 100035.

24 K. Shukla and V. C. Srivastava, *Can. J. Chem. Eng.*, 2018, **96**, 414–420.

25 N. Kumar, E. Leino, P. Mäki-Arvela, A. Aho, M. Käldström, M. Tuominen, P. Laukkanen, K. Eränen, J.-P. Mikkola, T. Salmi and D. Y. Murzin, *Microporous Mesoporous Mater.*, 2012, **152**, 71–77.

26 E. Leino, N. Kumar, P. Mäki-Arvela, A. Aho, K. Kordás, A.-R. Leino, A. Shchukarev, D. Y. Murzin and J.-P. Mikkola, *Mater. Chem. Phys.*, 2013, **143**, 65–75.

27 E. Leino, N. Kumar, P. Mäki-Arvela, A.-R. Rautio, J. Dahl, J. Roine and J.-P. Mikkola, *Catal. Today*, 2018, **306**, 128–137.

28 E. Leino, P. Mäki-Arvela, K. Eränen, M. Tenho, D. Y. Murzin, T. Salmi and J.-P. Mikkola, *Chem. Eng. J.*, 2011, **176–177**, 124–133.

29 E. Leino, P. Mäki-Arvela, V. Eta, N. Kumar, F. Demoisson, A. Samikannu, A.-R. Leino, A. Shchukarev, D. Y. Murzin and J.-P. Mikkola, *Catal. Today*, 2013, **210**, 47–54.

30 D. Ballivet-Tkatchenko, S. Chambrey, R. Keiski, R. Ligabue, L. Plasseraud, P. Richard and H. Turunen, *Catal. Today*, 2006, **115**, 80–87.

31 S.-J. Wang, S.-H. Cheng, P.-H. Chiu and K. Huang, *Ind. Eng. Chem. Res.*, 2014, **53**, 5982–5995.

32 S. Huang, P. Chen, B. Yan, S. Wang, Y. Shen and X. Ma, *Ind. Eng. Chem. Res.*, 2013, **52**, 6349–6356.

33 J. Wang, Z. Hao and S. Wohlrab, *Green Chem.*, 2017, **19**, 3595–3600.

34 A. Dibenedetto, M. Aresta, A. Angelini, J. Ethiraj and B. M. Aresta, *Chemistry*, 2012, **18**, 10324–10334.

35 B. Peng, H. Dou, H. Shi, E. E. Ember and J. A. Lercher, *Catal. Lett.*, 2018, **148**, 1914–1919.

36 Y. Yoshida, Y. Arai, S. Kado, K. Kunimori and K. Tomishige, *Catal. Today*, 2006, **115**, 95–101.

37 O. Arbeláez, A. Orrego, F. Bustamante and A. L. Villa, *Top. Catal.*, 2012, **55**, 668–672.

38 Y. Ikeda, M. Asadullah, K. Fujimoto and K. Tomishige, *J. Phys. Chem. B*, 2001, **105**, 10653–10658.

39 K. W. La, J. C. Jung, H. Kim, S.-H. Baeck and I. K. Song, *J. Mol. Catal. A: Chem.*, 2007, **269**, 41–45.

40 M. Honda, S. Kuno, N. Begum, K.-i. Fujimoto, K. Suzuki, Y. Nakagawa and K. Tomishige, *Appl. Catal., A*, 2010, **384**, 165–170.

41 M. Honda, M. Tamura, Y. Nakagawa, S. Sonehara, K. Suzuki, K.-i. Fujimoto and K. Tomishige, *ChemSusChem*, 2013, **6**, 1341–1344.

42 M. Honda, M. Tamura, Y. Nakagawa, K. Nakao, K. Suzuki and K. Tomishige, *J. Catal.*, 2014, **318**, 95–107.

43 K. Tomishige, H. Yasuda, Y. Yoshida, M. Nurunnabi, B. Li and K. Kunimori, *Green Chem.*, 2004, **6**, 206–214.

44 K. Tomishige, H. Yasuda, Y. Yoshida, M. Nurunnabi, B. Li and K. Kunimori, *Catal. Lett.*, 2004, **95**, 45–49.

45 M. Tamura, M. Honda, Y. Nakagawa and K. Tomishige, *J. Chem. Technol. Biotechnol.*, 2014, **89**, 19–33.

46 M. Honda, M. Tamura, K. Nakao, K. Suzuki, Y. Nakagawa and K. Tomishige, *ACS Catal.*, 2014, **4**, 1893–1896.

47 M. Honda, S. Sonehara, H. Yasuda, Y. Nakagawa and K. Tomishige, *Green Chem.*, 2011, **13**, 3406–3413.

48 M. Tamura, M. Honda, K. Noro, Y. Nakagawa and K. Tomishige, *J. Catal.*, 2013, **305**, 191–203.

49 M. Tamura, A. Miura, M. Honda, Y. Gu, Y. Nakagawa and K. Tomishige, *ChemCatChem*, 2018, **10**, 4821–4825.

This journal is © The Royal Society of Chemistry 2021

Catal. Sci. Technol., 2021, **11**, 1940–1948 | **1947**

50 K. Tomishige, M. Tamura and Y. Nakagawa, *Chem. Rec.*, 2019, **19**, 1354–1379.

51 Y. Gu, A. Miura, M. Tamura, Y. Nakagawa and K. Tomishige, *ACS Sustainable Chem. Eng.*, 2019, **7**, 16795–16802.

52 M. Tamura, K. Noro, M. Honda, Y. Nakagawa and K. Tomishige, *Green Chem.*, 2013, **15**, 1567–1577.

53 K. Tomishige, T. Sakaihori, Y. Ikeda and K. Fujimoto, *Catal. Lett.*, 1999, **58**, 225–229.

54 C. H. T. Tseng, B. K. Paul, C.-H. Chang and M. H. Engelhard, *Int. J. Adv. Des. Manuf. Technol.*, 2013, **64**, 579–586.

55 C. T. Nottbohm and C. Hess, *Catal. Commun.*, 2012, **22**, 39–42.

56 E. Leibnitz and H. G. Struppe, *Handbuch der Gaschromatographie*, Akademische Verlagsgesellschaft Geest & Portig K.-G., Leipzig, 1984.

57 A. M. D'Angelo, N. A. S. Webster and A. L. Chaffee, *Powder Diffr.*, 2014, **29**, S84–S88.

58 Y. F. Wu, X. H. Song, J. H. Zhang, S. Li, X. H. Yang, H. Z. Wang, R. P. Wei, L. J. Gao, J. Zhang and G. M. Xiao, *J. Taiwan Inst. Chem. Eng.*, 2018, **87**, 131–139.

59 P. Janoš, P. Kuráň, J. Ederer, M. Šťastný, L. Vrtoch, M. Pšenička, J. Henych, K. Mazanec and M. Skoumal, *Adv. Mater. Sci. Eng.*, 2015, **2015**, 241421.

60 P. Burroughs, A. Hamnett, A. F. Orchard and G. Thornton, *J. Chem. Soc., Dalton Trans.*, 1976, 1686–1698, DOI: 10.1039/DT9760001686.

61 M. Boaro, F. Giordano, S. Recchia, V. D. Santo, M. Giona and A. Trovarelli, *Appl. Catal., B*, 2004, **52**, 225–237.

62 D. Stoian, F. Medina and A. Urakawa, *ACS Catal.*, 2018, 3181–3193, DOI: 10.1021/acscatal.7b04198.

63 C. Schilling, M. V. Ganduglia-Pirovano and C. Hess, *J. Phys. Chem. Lett.*, 2018, **9**, 6593–6598.

64 C. Zhang, A. Michaelides, D. A. King and S. J. Jenkins, *Phys. Rev. B: Condens. Matter*, 2009, **79**, 075433.

65 L. Chen, S. Wang, J. Zhou, Y. Shen, Y. Zhao and X. Ma, *RSC Adv.*, 2014, **4**, 30968–30975.

66 P. H. Rana and P. A. Parikh, *New J. Chem.*, 2017, **41**, 2636–2641.

67 K. T. Jung and A. T. Bell, *J. Catal.*, 2001, **204**, 339–347.

68 B. Liu, C. Li, G. Zhang, X. Yao, S. S. C. Chuang and Z. Li, *ACS Catal.*, 2018, **8**, 10446–10456.

69 W. Wang, S. Wang, X. Ma and J. Gong, *Catal. Today*, 2009, **148**, 323–328.

70 Y. Wang, D. Jia, Z. Zhu and Y. Sun, *Catalysts*, 2016, **6**, 52.

71 T. Chang, M. Tamura, Y. Nakagawa, N. Fukaya, J.-C. Choi, T. Mishima, S. Matsumoto, S. Hamura and K. Tomishige, *Green Chem.*, 2020, **22**, 7321–7327.

72 Y. Pu, K. Xuan, F. Wang, A. Li, N. Zhao and F. Xiao, *RSC Adv.*, 2018, **8**, 27216–27226.

73 H. Liu, W. Zou, X. Xu, X. Zhang, Y. Yang, H. Yue, Y. Yu, G. Tian and S. Feng, *J. CO2 Util.*, 2017, **17**, 43–49.

74 M. Aresta, A. Dibenedetto, C. Pastore, C. Cuocci, B. Aresta, S. Cometa and E. Degiglio, *Catal. Today*, 2008, **137**, 125–131.

1948 | *Catal. Sci. Technol.*, 2021, **11**, 1940–1948

This journal is © The Royal Society of Chemistry 2021